

Optical properties of size fractions of suspended particulate matter in littoral waters of Quebec

Gholamreza Mohammadpour¹, Jean-Pierre Gagné¹, Pierre Larouche², Martin A. Montes-Hugo^{1*}

¹Institut des Sciences de la Mer de Rimouski, 310 Allée des Ursulines, Office P-216, Rimouski, Québec, Canada, G5L 3A1

5 ²Institut Maurice-Lamontagne, Pêches et Océans Canada, Mont-Joli, Québec, Canada, G5H 3Z4

Correspondence to: Martin A. Montes-Hugo (martinalejandro_montes@uqar.ca)

Abstract. Empirical mass-specific absorption ($a_i(\lambda)^*$) and scattering ($b_i(\lambda)^*$) coefficients of suspended particulate matter (SPM) were measured for four size fractions ($i = 0.2-0.4 \mu\text{m}$, $0.4-0.7 \mu\text{m}$, $0.7-10 \mu\text{m}$, and $>10 \mu\text{m}$, $\lambda =$ wavelength in nm) in surface waters (i.e., 0-5 m depth) of the Saint Lawrence Estuary and Saguenay Fjords (SLE-SF) and during June of 2013. The response of two optical proxies (the spectral slope of particulate beam attenuation coefficient and mass-specific particulate absorption coefficient, hereafter γ and S_{vis} , respectively) to changes on particle size and chemical composition was also examined. For the spectral range 400-710 nm, mass-specific absorption coefficients of total SPM (i.e., particulates $> 0.2 \mu\text{m}$) (hereafter a_{SPM}^*) had low values (i.e., $0.01-0.02 \text{ m}^2 \text{ g}^{-1}$) in areas of the lower estuary dominated by large-sized particle assemblages with relatively high particulate organic carbon and chlorophyll a per unit of mass. Conversely, largest a_{SPM}^* values (i.e., $> 0.5 \text{ m}^2 \text{ g}^{-1}$) corresponded with locations of the upper estuary and SF where particulates are relatively small-sized and/or mineral-rich. The differential Junge slope of particle size distribution had a larger correlation with b_i^* (Spearman rank correlation coefficient ρ_s up to 0.37) with respect to a_i^* (ρ_s up to 0.32). Conversely, the ratio between particulate inorganic matter and SPM concentration had a stronger influence on a_i^* (ρ_s up to 0.50). The magnitude of γ was sensitive to changes on size fractions of SPM mass, and the response of γ to particle composition variability was secondary. Lastly, in areas of the estuary with a larger marine influence (i.e., lower estuary), the magnitude of S_{vis} was inversely correlated with $a_{SPM}^*(440)$ values and the mineral content of SPM. Functionalities between S_{vis} and $a_{SPM}^*(440)$ distributions and unusual high values of a_i^* measured in SF waters suggest that iron bound to particles is likely a major factor explaining relatively high values of $a_{SPM}^*(440)$ in our study area.

1 Introduction

25 The distribution of suspended particulate matter (SPM) in coastal and estuarine environments has a major influence on several biogeochemical processes (e.g., phytoplankton blooms) (Guinder et al., 2009), ecosystem structure (e.g., food webs)

(Dalu et al., 2016) and dispersion of pollutants (e.g., copper, mercury, polycyclic aromatic hydrocarbons) (Ma et al., 2002; Ramalhosa et al., 2005). Light absorption by suspended particulates is essential for several photochemical processes related to the carbon cycle (e.g. photosynthesis, production of dissolved inorganic and organic carbon) (Estapa et al., 2012). Lastly, the concentration of SPM (CSPM) (Table 1) is an important variable for modeling thermodynamic processes and computing
5 heat budgets (Löptien and Meier, 2011) due to its influence on underwater light attenuation (Morel and Antoine, 1994; Devlin et al., 2008).

Remote sensing allows synoptic mapping of SPM in littoral environments where the spatial and temporal variability of suspended particulates is relatively high (Doxaran et al., 2002; Miller and McKnee, 2004; Montes-Hugo and Mohammadpour, 2012). However, ocean color algorithms for estimating CSPM will never have the accuracy required for
10 optical inversions because SPM is undefined optically (i.e., an unknown mixture of inorganic and organic matter). Therefore, partition of SPM into at least major chemical composition classes (particulate inorganic and organic matter or PIM and POM, respectively) and estimation of size distribution are required independently for optically-based remote sensing models of primary productivity and suspended mineral dynamics.

Likewise and unlike optical inversions of SPM, remote sensing estimates of specific fractions of SPM (e.g., PIM and POM)
15 have a definable and reproducible measurement error and are less influenced by regional variability of optical properties.

Despite this, there is still a lack of understanding regarding how SPM microphysical characteristics (e.g., particle chemical composition and size distribution) relate to mass-specific optical properties. This knowledge is essential for deriving new optical inversions for retrieving second-order attributes of SPM (i.e., chemical composition, size distribution).

Lastly, the biogeo-optical modeling of size and chemical fractions of SPM has a major scientific interest for understanding
20 the dynamics of different mineral iron forms in coastal waters (Estapa et al., 2012) as particle-associated iron has two specific light absorption bands (wavelength, $\lambda = 360-390$ nm and $\lambda = 400-450$ nm). Also, Estapa et al. (2012) demonstrated that optical proxies such as the spectral slope of particulate absorption (S_{vis}) within the visible spectral range ($\lambda = 400-700$ nm) could be used for estimating dithionite-extractable iron and organic carbon content in marine samples. Iron can be part of organic (e.g., complexed forms) or inorganic (e.g., silicate sheets) particulates having a broad size range (e.g., from clays
25 to amorphous aggregates) (Bettiol et al., 2008). Thus, the analysis of different fractions of SPM is essential for understanding the complex fate of iron in aquatic systems. Linking iron distributions with optical properties of size and chemical fractions of SPM may allow the development of proxies for mapping iron based on optical (*in water* and remote sensing) measurements. This is particularly advantageous for long-term monitoring projects as direct iron measurements are very expensive, difficult, and demand highly trained technicians.

30 The optical characterization of particle size distribution (PSD) and/or chemical composition in coastal and oceanic waters has been attempted based on four main methodologies: (1) analysis of spectral changes of inherent optical properties (Boss et al., 2001; Loisel et al., 2006), (2) empirical relationships between mass-specific optical cross sections and biogeo-physical characteristics of PIM (e.g., mean diameter) (Bowers et al., 2009) and SPM (e.g. apparent density of particulates) (Neukermans et al., 2012), (3) optical inversions of different volume scattering functions (Zhang et al., 2014), and (4)

changes on water leaving polarized reflectance (Loisel et al., 2008). A widely used methodology for estimating particle size spectra changes is the use of the spectral slope of particulate beam attenuation coefficient (γ) due to its relationship with the differential Junge slope of particle size distribution (ξ) (Boss et al., 2001).

The Saint Lawrence Estuary (SLE) and the Saguenay Fjords (SF) constitute a large sub-Arctic system characterized by relatively high concentrations of chromophoric dissolved organic matter (CDOM) (Nieke et al., 1997). The remote sensing of SPM microphysical characteristics in these waters is crucial for understanding regional climate effects on coastal erosion (Bernatchez and Dubois, 2004) and occurrence of harmful algae blooms (Fauchot et al. 2008). However, in order to accomplish this task it is essential to know how mass-specific optical coefficients of suspended particulates are influenced by particle composition and size distribution changes. To our knowledge, mass-specific absorption and scattering coefficients of SPM size fractions have never been reported in the literature even though it has a potential application in biogeo-optical inversions and biogeochemical studies regarding the dynamics of trace metals, sediment transport and primary productivity models.

This study has two main objectives: (1) to characterize the mass-specific absorption ($a_i(\lambda)^*$) and scattering ($b_i(\lambda)^*$) coefficients of four size fractions of SPM ($i = 0.2-0.4 \mu\text{m}$, $0.4-0.7 \mu\text{m}$, $0.7-10 \mu\text{m}$, and $>10 \mu\text{m}$, $\lambda =$ wavelength in nm) in different locations of the SLE-SF and during spring conditions, (2) to establish relationships between mass-independent optical coefficients calculated in (1) and microphysical properties of particulates related to PSD and mineral content of SPM, and (3) to examine the response of two optical proxies (γ and S_{vis}) to changes on PSD and chemical composition of SPM as inferred from PIM and POM contributions.

This study is organized in three sections. In the first section, mass-specific absorption (a_{SPM}^*) and scattering (b_{SPM}^*) coefficients of total SPM (i.e., particulates $>0.2 \mu\text{m}$) are calculated for different optical environments of the SLE-SF that are characterized by distinct particle assemblages and variable contributions of CDOM, non-algal particulates (NAP) and phytoplankton to light attenuation. In the second section, the response of mass-specific optical coefficients of different SPM size fractions to variations in PSD and mineral-content of suspended particulates is investigated. Lastly in the third section, the influence of PSD and mineral enrichment of particulates on γ and S_{vis} is examined.

2 Data and methods

2.1 Study area

The SLE can be divided in two main regions having contrasting biological productivity and bathymetry: the upper (UE) and the lower (LE) estuary (Levasseur et al., 1984). NAP and CDOM dominate the underwater light attenuation of UE waters (Nieke et al., 1997). This is in part related to the inflow of CDOM-rich and NAP-rich waters coming from the St. Lawrence River and Saguenay Fjord (Tremblay and Gagné, 2007; Xie et al., 2012). Unlike NAP and CDOM, contribution of phytoplankton to inherent optical properties increases towards the mouth of the SLE (Montes-Hugo and Mohammadpour, 2012; Xie et al., 2012).

The study of optical properties of suspended particulates in SLE waters began during the late 80's. Babin et al. (1993) investigated the horizontal variability of the specific absorption coefficient of phytoplankton (i.e., absorption coefficient normalized by concentration of chlorophyll + phaeopigments) in surface waters during summer of 1989 and 1990. During the summer of 1990, Nieke et al. (1997) studied the spatial variability of CDOM in terms of fluorescence and absorption spectra. Also, this study reported for the first time relatively high (up to 3 m^{-1}) particulate beam attenuation coefficients (c_{SPM}) and inverse relationships between salinity, c_{SPM} , and CDOM absorption coefficients (a_{CDOM}). Larouche and Boyer-Villemaire (2010) proposed remote sensing models for estimating PIM in the SLE and the Gulf of Saint Lawrence. Xie et al. (2012) showed inverse relationships between salinity and absorption coefficients of NAP and highlighted the extremely high values of a_{CDOM} (i.e., up to 5.8 m^{-1} at $\lambda = 412 \text{ nm}$) along the Saguenay Fjord.

10 Historical studies performed during summer of 1975 suggest that size distribution of SPM differs between UE, LE and SF regions (Poulet et al., 1986). Based on surface samples, Poulet et al. (1986) found a dominance of relatively 'small-sized' (i.e., mode diameter $< 10 \text{ }\mu\text{m}$) and 'large-sized' (i.e., $> 30 \text{ }\mu\text{m}$) particulates over the UE and the mouth of the SLE, respectively. Conversely, the remaining locations of the LE were characterized by particulates having an intermediate size. In surface waters of SF and during spring months, SPM is commonly composed by very small particles (i.e., $2\text{-}3 \text{ }\mu\text{m}$)

15 (Chanut and Poulet, 1979). Several investigations point out that suspended particulates in SLE-SF regions are principally composed by inorganic matter (D'Anglejan and Smith, 1973; Larouche and Boyer-Villemaire, 2010). This mineral contribution varies between 60 and 95% of dry weight depending on the geographic location and period of the year (Yeats, 1988; Larouche and Boyer-Villemaire, 2010). Despite their important contribution, none of these studies reported mass-normalized optical coefficients for different size fractions of SPM nor an assessment of particle composition and size

20 distribution effects on these coefficients.

2.2 Field surveys

Discrete water samples for biogeochemical and optical measurements were obtained in 22 locations distributed throughout the SLE ($N = 17$) and SF ($N = 5$) regions (Fig. 1). One discrete sample was obtained in each sampling locations but in site 6 where 2 measurements were made during June 3 and 6 of 2013. Samples corresponding to a sampling depth of 0-2 m were

25 collected during June 3-9 of 2013 by using an oceanographic rosette equipped with Niskin bottles (volume = 12 L). For each sampling location, mass of different size fractions of SPM, optical coefficients for different SPM size fractions, and particle size distribution spectra were measured inside the wet lab of the vessel.

2.3 Biogeochemical analysis

Size fractionation of SPM was done after sequentially filtering the original samples through pre-weighted membranes having

30 a diameter of 47 mm and a pore size of $10 \text{ }\mu\text{m}$ (Whatman, polycarbonate), $0.7 \text{ }\mu\text{m}$ (GF/F, Whatman, glass fiber), $0.4 \text{ }\mu\text{m}$ (Whatman, polycarbonate), and $0.2 \text{ }\mu\text{m}$ (Nucleopore, polycarbonate). The contribution of size fraction i to the total mass of SPM (F_{SPM}^i , $i = 0.2\text{-}0.4 \text{ }\mu\text{m}$, $0.4\text{-}0.7 \text{ }\mu\text{m}$, $0.7\text{-}10 \text{ }\mu\text{m}$, and $>10 \text{ }\mu\text{m}$) was computed by normalizing the weight of the fraction i

by the sum of weights derived from each size fraction. The mineral and organic composition of suspended particulates (F_{SPM}^j , where j superscript symbolizes PIM or POM, respectively) was only computed for particulates with a grain size greater than $0.7 \mu\text{m}$ (i.e., after filtering the original unfractionated sample through a GF/F filter membrane). In this case, the mass of PIM and POM was assumed to be negligible for particulates with a diameter smaller than $0.7 \mu\text{m}$. Thus, resulting

5 PIM and POM determinations correspond to total suspended particulates. This approximation should be verified in the future since the authors are not aware of publications addressing the contribution of relatively small particulates (i.e., $< 0.7 \mu\text{m}$) to PIM and POM. The mass of PIM was obtained after removing the organic mass (i.e., POM) by combustion of original samples at 450°C and during 6 h (Mohammadpour et al., 2015). The mass of POM was calculated as the difference between the dry mass of particulates concentrated in GF/F filters minus the dry mass of PIM.

10 The precision of SPM mass determinations based on GF/F filters was 15% (Mohammadpour et al., 2015). This precision was computed as the percentage of ± 1 standard deviation with respect to the arithmetic average of weight corresponding to 10 replicas. Based on loss on ignition factors (Barillé-Boyer et al., 2003) and clay composition data obtained in the Saint Lawrence Estuary (D'Anglejan and Smith, 1973), the estimated error of PIM determinations due to dehydration of clays was 3.1%. Thus, PIM mass determinations have a maximum uncertainty of 18.1% due to the additional error of SPM mass

15 measurements by gravimetry. Notice that error in POM mass estimates was slightly greater than that associated to PIM mass estimates (18.2%).

2.4 Optical measurements

Total absorption (a) and beam attenuation (c) coefficient measurements were done on unfiltered and size-fractionated filtered water samples previously described in section 2.3. Discrete samples for optical coefficients were measured onboard by using

20 an absorption-beam attenuation meter (ac-s, WetLabs, $\lambda = 400.3\text{-}747.5 \text{ nm}$, average spectral resolution = 4 nm, path-length = 10 cm, accuracy $\pm 0.001 \text{ m}^{-1}$). In order to minimize the presence of bubbles, a pump (ISMATEC MCP-Z) was used to gently circulate the samples through the ac-s tubes. Spikes on raw signal associated to bubbles were removed by visual inspection. Residual scattering on absorption measurements was removed by applying a flat baseline at a reference wavelength of 715 nm (Bricaud and Stramski, 1990). This is a first order correction for scattering effects on non-water absorption coefficient

25 estimates. Thus, the calculation of particulate absorption coefficients in this study is expected to have a bias with respect to true values measured using absorption-meter instruments that are less influenced by particulate scattering (e.g., point-source integrating-cavity absorption meters) (Röttgers et al., 2013). Lastly, values of a and c were corrected by water temperature and salinity variations (Pegau et al. 1997). Spectral values of a_{SPM} in m^{-1} were derived in unfiltered samples by subtracting a_{CDOM} and the absorption coefficient for pure seawater (a_w) to a at each wavelength. The contributions $a_{CDOM} + a_w$ were

30 measured by using the a -tube (i.e., reflective tube) of the ac-s and after pre-filtration of total samples through a membrane having a pore size of $0.2 \mu\text{m}$ (nucleopore, Whatman). Similar to a_{SPM} calculations, the magnitude c_{SPM} was computed in unfiltered samples after subtracting CDOM and pure seawater contributions to c as derived by using the c -tube (i.e., opaque

tube) of the ac-s instrument. Notice that pure seawater contributions to a and c values are removed when the ac-s instrument is calibrated by the manufacturer. Lastly, particulate scattering coefficients (b_{SPM}) in m^{-1} were derived by subtracting a_{SPM} to c_{SPM} values.

The particle size spectra within the size range 3-170 μm were measured on unfiltered samples and by using a red laser (wavelength = 670 nm) diffractometer (LISST-100X, type B, Sequoia Scientifics) (Agrawal et al. 1991). LISST bench determinations were discrete and performed on board of the ship. Lab measurements were performed by using a chamber and a magnetic stir bar in order to homogenize the samples and avoid sinking of particulates. The optical path was covered with a black cloth to minimize ambient light contamination during the scattering measurements. The LISST-100X instrument can measure 32 scattering angles within an angular range of 0.08-13.5°, thus, particulates with a diameter between 1.25 and 250 μm can be quantified. However only the interval 3-170 μm was analyzed due to variability of particle shape and refractive index in the first bins (i.e., < 3.2 μm) (Agrawal et al., 2008; Andrews et al., 2010), stray light effects in the first bins (Reynolds et al. 2010), and bias related to particle sinking in the last bin (i.e., 170-250 μm) (Reynolds et al. 2010). Measurements were made during a period of 3 minutes at 1 Hz, and resulting raw data were quality controlled by using the Hampel filter algorithm for eliminating outliers (Pearson, 2005). The number of particles per unit of volume within each size class ($N(D)$) was computed by dividing the particle volume concentration ($V(D)$) by the diameter (D) of a volume-equivalent sphere for the midpoint of each individual class:

$$N(D) = 6 V(D) (\pi D^3)^{-1} \quad (1)$$

A total of 25 particle size bins were calculated based on inversions of the scattering pattern and by applying an inversion kernel matrix derived from scattering patterns of spherical homogenous particles as predicted from Mie theory and a realistic range of index of refraction. The particle size distribution ($N'(D)$) was defined as the average number of particles within a given size class of width ΔD and per unit of volume (Reynolds et al., 2010):

$$N'(D) = N(D) \Delta D^{-1} \quad (2)$$

The parameter ξ was computed as the exponent of the following power-type function:

$$N'(D) = N'(D_0) (D/D_0)^{-\xi} \quad (3)$$

where D_0 is the reference particle diameter and was set to 35.17 μm because is the midpoint of the size logarithmic size range. Calculations of ξ were done by least square minimization of log-transformed data (Reynolds et al., 2010). The uncertainty of ξ calculations, as estimated from 2 standard errors, varied between 1.6 and 10.2% with smaller errors in samples obtained in LE locations. Although particle size distribution in natural waters may not follow a Junge-type slope, its use here was justified since our main interest was to have a first-order assessment of size effects of particulates on optical coefficient's variability. Indeed, the definition of ξ based on LISST measurements applies for particulates greater than 2 μm . A more realistic representation of PSD is the model proposed by Risovic (1993). This parameterization mainly includes two particle populations ('large' and 'small') having different refractive index and has been recently applied in littoral

environments by different studies (Zhang et al., 2013; Zhang et al., 2014; Zhang et al., 2017). Thus, relationships between ξ and optical coefficients in this study are local and should not be generalized to other littoral environments.

2.5 Optical proxies and particle microphysical characteristics

The parameter γ is positively correlated with the exponent of the particle number size distribution ($\xi = \gamma + 3 - 0.5 e^{-6\gamma}$, Boss et al., 2001) and negatively related with the mean particle size for particles smaller than 20 μm (Boss et al., 2013). The parameter γ was derived as the exponent of a power-type regression model of c_{SPM} as a function of wavelength:

$$c_{\text{SPM}}(\lambda) = c_{\text{SPM}}(488) (\lambda/\lambda_r)^{-\gamma} \quad (4)$$

where $\lambda_r = 488$ nm and it is the reference wavelength (Boss et al., 2013).

The uncertainty of γ determinations varied between 2.2% and 6.4% with largest errors for samples obtained in LE waters. The spectral slope of empirical mass-specific particulate absorption coefficients (S_{vis}) was calculated by nonlinear fitting of a single-exponential decay function over the visible range 400-700 nm:

$$a_x^*(\lambda) = A e^{-S_{\text{vis}}(\lambda-400)} + B \quad (5)$$

where x corresponds to total SPM or the size class i , the term B corresponds to an offset at near-IR wavelengths to account for nonzero absorption by mineral particles (Babin et al. 2003; Röttgers et al., 2014). The uncertainty of S_{vis} estimates varied between 0.5 and 21.5% with largest errors corresponding with samples obtained in LE locations. The equation (5) is valid in waters where non-algal particulates are the main optical component contributing to light absorption coefficient of SPM. The magnitude of S_{vis} is inversely correlated with extractable iron from crystalline and amorphous iron oxides and organic-iron complexes in measurements corresponding to marine samples (Estapa et al., 2012). Also for the same environments, S_{vis} is expected to have a negative covariation with the organic carbon content of particulates (Estapa et al., 2012).

2.6 Mass-specific optical coefficients

Spectral values of mass-specific absorption ($a_i^*(\lambda)$) and scattering ($b_i^*(\lambda)$) coefficients in $\text{m}^2 \text{g}^{-1}$ and for different size fractions of SPM were calculated as:

$$a_i^*(\lambda) = a_i(\lambda) (\text{wp}_i)^{-1} \quad (6)$$

$$b_i^*(\lambda) = b_i(\lambda) (\text{wp}_i)^{-1} \quad (7)$$

For each size class i , a_i and b_i are the coefficients of particulate absorption and scattering, respectively, and wp_i is the mass of particulates per unit of volume in g m^{-3} .

2.7 Statistical analysis

The influence of particle size and chemical composition variations on empirical mass-specific optical coefficients of particulates for different size fractions (i.e., a_i^* and b_i^*) and optical proxies (γ and S_{vis}) was investigated based on

correlations with respect to ξ and $F_{\text{SPM}}^{\text{PIM}}$ variables, respectively. In all cases, the intensity and sign of correlations were quantified based on non-parametric Spearman rank coefficient (ρ_s) (Spearman, 1904).

3 Results

3.1 Spatial variability of microphysical properties of SPM

5 In terms of particle size distribution, contrasting areas in the SLE-SF were identified. In general, particulates with a diameter larger than 10 μm had a relatively large contribution to the total SPM mass in UE locations ($F_{\text{SPM}}^{>10\mu\text{m}}$ as percentage up to 17%). This proportion was lower in the LE (up to 11%) and SF (up to 15%) subregions. The largest mass contribution of smallest-sized particulates (i.e., diameter $< 0.4 \mu\text{m}$) was calculated in the lower estuary (up to 27%). Lastly, the intermediate size classes 0.4-0.7 μm and 0.7-10 μm were in average the fractions having the largest mass contributions to SPM in SF
10 locations (up to 14 and 87%, respectively). In general, the Junge slope calculations suggested the presence of relatively larger particulates in the LE (arithmetic average \pm standard deviation = 3.28 ± 0.38 , $N = 15$) with respect to UE (3.46 ± 0.36 , $N = 3$) and SF (3.42 ± 0.39 , $N = 5$) subregions. Unlike PSD, chemical composition of SPM was less variable throughout the study area ($F_{\text{SPM}}^{\text{PIM}}$ range = 37 to 87 %). In average, particle composition in UE, SF and LE subregions was dominated by minerals ($F_{\text{SPM}}^{\text{PIM}} = 0.65 \pm 0.13$, 0.67 ± 0.14 and 0.67 ± 0.14 for SF, UE and LE, respectively).

15 3.2 Mass-specific optical properties of SPM

For the spectral interval 400-710 nm, the magnitude of regionally-averaged a_{SPM}^* was higher in SF (e.g., for at $\lambda = 440 \text{ nm}$, arithmetic average \pm standard error = $0.523 \pm 0.102 \text{ m}^2 \text{ g}^{-1}$) with respect to UE ($0.122 \pm 0.068 \text{ m}^2 \text{ g}^{-1}$) and LE ($0.050 \pm 0.010 \text{ m}^2 \text{ g}^{-1}$) locations (Fig. 2a). Conversely, regionally-averaged b_{SPM}^* values were highly variable within spatial domains even though highest and lowest values tend to be associated with UE ($0.499 \pm 0.278 \text{ m}^2 \text{ g}^{-1}$) and LE ($0.129 \pm 0.046 \text{ m}^2 \text{ g}^{-1}$)
20 locations, respectively (Fig. 2b). In general for all size fractions of SPM, mass-specific absorption coefficients tended to be higher in SF (e.g., at $\lambda = 440 \text{ nm}$, up to $2.81 \text{ m}^2 \text{ g}^{-1}$) with respect to other subregions of the SLE (up to $2.11 \text{ m}^2 \text{ g}^{-1}$) (Fig. 3a). However for the smallest size range 0.2-0.4 μm , highest a_i^* values were measured in UE waters (e.g., st 14) ($2.19 \text{ m}^2 \text{ g}^{-1}$) (Fig. 3a). Spectral curves with the highest a_i^* values (e.g., up to $4 \text{ m}^2 \text{ g}^{-1}$ at $\lambda = 400 \text{ nm}$) corresponded with the smallest-sized and largest-sized fractions of SPM (Fig. 3a,d). These values were up to 8 and 5 times higher than those characteristic of size
25 fractions 0.4-0.7 μm and 0.7-10 μm , respectively (Fig. 3b-c). Similar to a_i^* , highest b_i^* values (up to $5.70 \text{ m}^2 \text{ g}^{-1}$ at $\lambda = 400 \text{ nm}$) were computed in size-fractionated samples corresponding to particle size ranges of 0.2-0.7 μm and $>10 \mu\text{m}$ (Fig. 4). Highest scattering efficiencies in terms of b_i^* were not always measured in the same region. Indeed, maximum b_i^* values for size fraction 0.7-10 μm (up to $1.25 \text{ m}^2 \text{ g}^{-1}$ at $\lambda = 556 \text{ nm}$) and $>10 \mu\text{m}$ (up to $4.58 \text{ m}^2 \text{ g}^{-1}$) were obtained in UE and LE domains, respectively. Notice that mass-specific optical coefficients in the near-Infrared (NIR) spectral range are not shown
30 due to the presence of negative values at some wavelengths.

Spectral variability of mass-specific optical coefficients for two size fractions of SPM and averaged over the whole study area is illustrated in Fig. 5. For the spectral range of 440-556 nm, a_i^* values for the size range 0.2-0.4 μm tended to be higher with respect to those associated with the particulates larger than 10 μm (Fig. 5a). Conversely, this trend appeared to be reversed at wavelengths within the red-NIR spectral range. In general for the visible-NIR wavelengths, the arithmetic average of b_i^* for the size fraction 0.2-0.4 μm were larger with respect to that associated to the size fraction >10 μm (Fig. 5b).

The subregional variation of mass-specific optical coefficients for different size fractions of SPM are depicted in Fig. 6. For all size fractions of SPM, the regionally-averaged magnitude of $a_i^*(440)$ was higher in UE-SF with respect to LE locations (Fig. 6a). These differences are consistent with spatial changes of a_{SPM}^* in Fig. 2a and 3. In Saguenay Fjord waters, the maximum regionally-averaged $a_i^*(440)$ values (up to 4.6 $\text{m}^2 \text{g}^{-1}$) were associated with the size fraction of SPM having particulates with a size grain larger than 10 μm (Fig. 6a). In general, ξ and $F_{\text{SPM}}^{\text{PIM}}$ correlations with mass-specific optical coefficients of different size fractions of SPM suggest that particle chemical composition has a larger influence on $a_i^*(440)$ (ρ_s up to 0.50, $P = 0.0009$) with respect to particle size (ρ_s up to 0.32, $P = 0.0033$) (Table 2).

Geographically-averaged $b_i^*(550)$ values were generally comparable among subregions (Fig. 6b). However for the size fraction 0.7-10 μm , averaged $b_i^*(550)$ values of UE-SF (0.432-0.501 $\text{m}^2 \text{g}^{-1}$) domains were larger with respect to the arithmetic average computed for LE waters (0.136 \pm 0.027 $\text{m}^2 \text{g}^{-1}$). Unlike $a_i^*(440)$, $b_i^*(550)$ variability was less influenced by changes on particle composition (ρ_s up to 0.42, $P = 0.0015$) (Table 2). Conversely, the impact of changing particle dimensions, as inferred from ρ_s correlations, was greater for $b_i^*(550)$ (ρ_s up to 0.37, $P = 0.006$) with respect to $a_i^*(440)$ (ρ_s up to 0.32, $P = 0.009$) values.

20 3.3 Optical proxies

Correlations between size and chemical fractions of SPM, as derived from mass ratios, and optical proxies are presented in Table 3. Over the whole study area, there was not a clear relationship between γ and chemical fractions of SPM fractions ($\rho_s = -0.34$, $P = 0.11$). However, γ responded to variations on size fractions for the range 0.2-10 μm (ρ_s up to 0.53, $P = 0.01$). The sign of this response changed depending on the size class under investigation (e.g., positive for small-sized, negative for intermediate-sized particulates). Although positively correlated, there was not a clear relationship between γ and ξ determinations ($\rho_s = 0.15$, $P = 0.49$, $N = 23$). The range of γ values was 0.759-3.282, 1.389-1.534, 2.873-3.282 and 0.759-1.802 nm^{-1} for the SLE, UE, SF and UE domains, respectively. The spectra slope of a_{SPM}^* was not substantially affected by $F_{\text{SPM}}^{\text{PIM}}$ changes ($\rho_s = -0.06$, $P = 0.78$, $N = 23$), however S_{vis} variability was strongly influenced by particle size changes (Table 3). Also, size effects on S_{vis} were more remarkable for relatively small-sized particulates (i.e., 0.2-0.7 μm). This pattern was consistent with a positive correlation between γ and S_{vis} ($\rho_s = -0.489$, $P = 0.018$, $N = 23$). However, there was not a clear relationships between S_{vis} and ξ ($\rho_s = 0.123$, $P = 0.57$, $N = 23$).

Range of S_{vis} values of total SPM was 0.005-0.051, 0.009-0.017, 0.014-0.051 and 0.005-0.016 nm^{-1} for the SLE, UE, SF and UE domains, respectively. Over the whole study area, the range of S_{vis} values was 0.004-0.026, 0.007-0.052, 0.004-0.109 and 0.001-0.028 nm^{-1} for size fractions 0.2-0.4 μm , 0.4-0.7 μm , 0.7-10 μm and $> 10 \mu\text{m}$, respectively. In general, S_{vis} slopes were not correlated between size fractions even though the magnitude of S_{vis} for total SPM was strongly influenced by S_{vis} calculated for the 0.7-10 μ fraction ($\rho_s = 0.66$, $P = 0.004$).

4 Discussion

4.1 Uncertainty of optical measurements

Inherent optical properties in this study were derived from an ac-s instrument. Thus, large errors on absorption coefficients may be anticipated in relatively turbid waters if original measurements are not corrected by scattering effects (Boss et al., 2009; McKee et al., 2013). These effects are mainly attributed the acceptance angle of the transmissometer and the multiple scattering of photons. The acceptance angle of the ac-s instrument is $\sim 0.9^\circ$ and much larger than that corresponding to the LISST-100X diffractometer ($\sim 0.027^\circ$). Thus, a larger underestimation on c magnitude is expected in ac-s with respect to LISST-100X measurements due to a larger contribution of forward-scattered photons arriving to the detector of the former optical instrument. Further comparisons of $c(532)$ measurements derived here by ac-s and LISST-100X showed that c values as derived from ac-s were 23-84% lower with respect to those determinations based on LISST-100X. This is consistent with Boss et al. (2009) who reported that uncorrected Wet Labs ac-9 attenuation values are approximately 50%-80% of equivalent LISST attenuation data. Unfortunately, c deviations due to acceptance angle variations were not corrected in this study due to the lack of true c values as obtained by using an integrating cavity absorption meter (e.g., PSICAM) (Röttgers et al., 2005). Notice that these errors are much greater with respect to the optical variability associated to each sample determination in SLE-SF waters and computed based on ac-s measurements (e.g., $< 1\%$ at $\lambda = 532 \text{ nm}$).

In this investigation, the 'flat' baseline correction was selected for correcting residual scattering in absorption coefficient estimates as derived from ac-s measurements. This technique was chosen due to the lack of PSICAM measurements or critical ancillary optical information (e.g., particle backscattering efficiency) to tune up a Monte Carlo scattering correction approach (McKee et al., 2008). The 'flat' scattering correction approach is expected to provide a fair correction of a values in oceanic waters (up to 15% underestimation at wavelengths shorter than 600 nm, see Fig. 8b, McKnee et al., 2013) but may result in large deviations (up to 100% decrease in the NIR spectral range) of a values in relatively turbid waters (e.g., $a > 0.2 \text{ m}^{-1}$) such as the Baltic/North Sea. Also, this issue is present when the proportional correction method of Zaneveld et al. (1994) is applied. Unlike the 'flat' baseline, the scattering residual of the proportional method is spectrally dependent but still relying in one reference wavelength in the NIR spectral range. Approximations justifying the use of the 'flat' (i.e., zero absorption signal in the NIR) and 'proportional' (i.e., wavelength-dependent scattering phase function) method are still in debate (McKnee et al., 2013). Lastly, the Monte Carlo correction method (McKee et al., 2008) has in general better

agreement (error <10%) with true a values as derived from an integrating cavity absorption meter. However, this approach may also have major uncertainties due to assumptions regarding optical coefficients (e.g., particulate backscattering ratio and volume scattering function) and changes on scattering efficiency by the inner wall of the reflective tube due to aging (McKnee et al., 2013). Thus in conclusion, the resulting optical coefficients and mass-specific optical coefficients of
5 particulates measured in SLE-SF waters may present large errors (i.e., > 50%) with respect to true values and at wavelengths longer than 550 nm. This bias is anticipated to be maximum (minimum) in UE (LE) locations.

4.2 Variability of microphysical properties of SPM

A striking finding in this study was the important weight contribution of relatively large particulates (i.e., >10 μm) in UE waters. This phenomenon was likely attributed to the active resuspension of sediments associated with vertical mixing
10 produced by tidal currents and winds (Yeats, 1988). Conversely, this effect was secondary in relatively deep waters of SF and LE where large and heavy particulates are rapidly removed from the water column and deposited along submarine canyons (Gagné et al., 2009). Although chemical composition of size-fractionated SPM was not analyzed in this study, additional correlations with $F_{\text{SPM}}^{\text{PIM}}$ suggest that particulates smaller than 10 μm were richer in inorganic matter ($\rho_s = 0.62$, $P < 0.001$, $N = 23$) with respect to particulates with a diameter greater than 10 μm . This finding confirms previous studies
15 showing that relatively small ($\sim 2 \mu\text{m}$) particulates in the SLE are mainly composed by minerals (Yeats, 1988; Gagné et al., 2009). In this contribution, a large proportion of particulates with a diameter above 50 μm and lower ξ values were typically found in LE locations. These results also support historical observations made during July and August and showing a greater proportion of relatively large particulates (i.e., > 5 and < 50 μm) over the LE locations (Chanut and Poulet, 1979).

4.3 Spatial variability of mass-normalized optical coefficients

In this study, a_{SPM}^* measurements in the visible and near-IR range had a large variability that was comparable to the range of values reported in the literature for temperate coastal waters (e.g., Mobile Bay, River of La Plata, Elbe Estuary, Gironde Estuary) (Stavn and Richter, 2008; Doxaran et al., 2009) (Table 4). This is remarkable given the large diversity of methodologies used to estimate a_{SPM}^* and b_{SPM}^* values. In general, lowest a_{SPM}^* values (i.e., 0.01-0.02 $\text{m}^2 \text{g}^{-1}$ at $\lambda = 440 \text{ nm}$) commonly corresponded with samples obtained in very turbid environments (i.e., > 100 g m^{-3} , Mississippi River and Delta,
25 Gironde River, La Plata River) (Bowers and Binding, 2006; D'Sa et al. 2006; Doxaran et al., 2009). Notice that part of this decrease can be attributed to an incomplete removal of multiple scattering effects. Relative low a_{SPM}^* values have been linked to high POC/SPM (Wozniak et al., 2010) and chl/SPM concentration ratios, where chl means chlorophyll a concentration (Estapa et al., 2012). In this study, chl/SPM presented values as high as $2 \cdot 10^{-3}$ that are comparable to relatively high ratios reported by D'Sa et al. (2006). Thus, it is suggested that some locations in our study area are characterized by
30 relatively high POC/SPM as other turbid coastal environments such as adjacent waters to the Mississippi Delta (D'Sa et al. 2006).

A well-known mechanism explaining the general decrease of a_{SPM}^* in very turbid waters is related to packaging effects (Morel, 1974; Zhang et al., 2014). At higher turbidities, larger particulates contribute to PSD variations, thus as mean diameter of particles increases, the light absorption efficiency per averaged particle decreases (i.e., the interior of larger particles has a greater ‘shading’). This could also explain the spatial differences of $a_{\text{SPM}}^*(440)$ in our study area where larger values corresponded with surface waters dominated by particles assemblages having a smaller mean diameter (i.e., UE and SF). In nearshore waters of California, Wozniak et al. (2010) demonstrated inverse relationships between $a_{\text{SPM}}^*(440)$ and the median particle diameter for inorganic- and organic-dominated assemblages. Also and consistent with our previous discussion regarding particle composition, Wozniak et al. (2010) observed that POC/SPM was positively correlated with the median particle diameter. Indirect size effects on $a_{\text{SPM}}^*(440)$ due to changes on iron content per particle have been discussed by Estapa et al. (2012) in environments where optical properties are dominated by NAP. In general, smaller particulates have a greater surface for adsorbing organic compounds where iron can accumulate (Mayer, 1994; Poulton and Raiswell, 2005). Thus, SPM fractions with smaller particulates are expected to have an enhancement of $a_{\text{SPM}}^*(440)$ due to relatively high iron concentrations. This phenomenon likely explained our higher $a_{\text{SPM}}^*(440)$ in SF regions with respect to LE waters where the water salinity range is 0-29 and 29-33.5, respectively (El Sabh, 1988). Indeed, relatively high concentrations of iron bound to particulates have been measured in surface waters of the Saguenay Fjord (Yeats and Bewers, 1976; Tremblay and Gagné, 2009). In coastal Louisiana and the lower Mississippi and Atchafalaya rivers, Estapa et al. (2012) found that magnitude of a_{SPM}^* within the UV ($\lambda \sim 360\text{-}390$ nm) and blue ($\lambda \sim 400\text{-}450$ nm) spectral range is commonly higher in freshwater with respect to marine samples. This difference was related to the greater concentration of particulate iron oxides and hydroxides derived from terrestrial sources in freshwater samples and later transport and reduction in marine environments. Notice that unlike our study, Estapa et al. (2012) used a different method for measuring a_{SPM}^* and based on absorbance changes inside an integrating sphere. Iron oxide and hydroxide minerals have a major light absorption within the spectral range of 400-450 nm due to the absorption bands of iron (Estapa et al., 2012). Pigmentation of mineral particulates due to iron hydroxides has been suggested to be a major factor increasing a_{SPM}^* (Babin and Stramski, 2004; Estapa et al., 2012). Unfortunately, no chemical determinations of iron hydroxides were performed during our study in order to test these relationships. Likewise and unlike optical measurements made by Estapa et al. (2012), the resolution of our ac-s measurements (~ 4 nm) did not allow a quantification of iron bound to particulates.

Similar to a_{SPM}^* , b_{SPM}^* values were highly variable between locations and within the range of measurements obtained in other environments (Table 4). In this study, the spectral variation b_{SPM}^* between regions showed a spectral flattening as particle assemblages become dominated by organic matter (i.e., LE). This finding is consistent with Wozniak et al. (2010) measurements made in Imperial Beach, California.

4.4 Particle size and chemical composition effects on mass-specific optical coefficients

Correlations of ξ and $F_{\text{SPM}}^{\text{PIM}}$ with mass-specific optical coefficients for different SPM size fractions were shown in Table 2. For all size fractions, ξ was positively correlated with $a_i^*(440)$ (ρ_s up to 0.32, $P = 0.006$). This pattern suggests a higher

absorption efficiency of relatively small-sized particulates. As previously discussed, these particulates have a greater light absorption per unit of particle mass due to a lesser role of shading effects and presumably a greater iron-enrichment. Since particle aggregates were altered during our experiments, the influence of particle density on mass-specific optical coefficients cannot be quantified as this effect is mainly observed in undisrupted marine aggregates (Slade et al. 2011; 5 Neukermans et al., 2012, Neukermans et al 2016). However and based on Estapa et al. (2012) simulations, the impact of aggregation on a_{SPM}^* is anticipated to be small (i.e., ~10%) with respect to the spatial variability of a_{SPM}^* in SLE-SF waters. In general, ξ was positively correlated with b_i^* (550) (ρ_s up to 0.37, $P = 0.008$) and pointed out as expected an increase of scattering efficiency as particulates become smaller and the influence of packaging effects is less important. Notice that ξ correlations with b_i^* (550) were greater with respect to a_i^* (440) and more remarkable for relatively large-sized particulates. In 10 Arctic waters, Reynolds et al. (2016) observed an increase on mass-specific particulate backscattering for mineral-rich particle assemblages that tend to exhibit steeper size distributions. Although no particulate backscattering measurements were available in this study, Reynolds et al. (2016) highlight the importance of relatively small-sized particulates for driving variations on mass-specific optical coefficients linked to scattering processes.

In all cases, F_{SPM}^{PIM} had a stronger correlation with a_i^* (440) compared with b_i^* (550) values, and these relationships were 15 stronger when SPM was dominated by particulates with an intermediate size (i.e., 0.4-10 μm). The enrichment of suspended particulates on inorganic matter and concomitant variations a_i^* (440) may be explained by a greater contribution of mineral-associated iron to light absorption. Also, the combustion method used to measure PIM in our study could be another factor explaining the increased particle absorption in the blue range (Babin et al. 2003). Iron can take many forms in mineral particulates (oxides, hydroxides, monosulfides) and can be deposited over the particle surface or be part of its internal 20 structure (e.g., clays). Since the mean diameter of clay particles is less than 2 μm , the aforementioned F_{SPM}^{PIM} - a_i^* (440) correlations were also likely affected by iron associated (adsorbed or structural) to other types of inorganic particulates that are characterized by larger dimensions. In SF locations, reduced iron is mainly associated to dissolved organic compounds that can be strongly adsorbed to hydrous metal oxides (Deflandre et al., 2002). Babin and Stramski (2004) obtained positive correlations between a_{SPM}^* and iron content of dust and soil particles suspended in seawater. Estapa et al. (2012) found a 25 strong covariation between a_{SPM}^* values and dithionite-extractable iron content of oxides and hydroxides.

An important objection to correlations of ξ and F_{SPM}^{PIM} with mass-specific optical coefficients of SPM size fractions was related to differences in terms of particle size range used to compute ξ and F_{SPM}^{PIM} and particle size classes derived by sequential filtration of water samples. More specifically, ξ is not representative of submicron particles less than 2 μm . Also, F_{SPM}^{PIM} is only a valid particle composition parameter for particles mostly larger than 0.7 μm . Thus, correlations ξ and 30 F_{SPM}^{PIM} with mass-specific optical coefficients of 0.2-0.4 μm and 0.4-0.7 μm may only reflect indirect dependencies between mass-normalized optical coefficients of different size classes. This possibility (i.e., correlations between a_i^* or b_i^* of different size classes) was confirmed based on samples obtained in UE, LE and SF waters. Lastly, it is important to discuss the potential bias on a_i^* and b_i^* determinations due to size fractionation and *a posteriori* impact on correlations with respect to

F_{SPM}^{PIM} and ξ values. No measurements of F_{SPM}^{PIM} and ξ were done in size fractions of SPM, thus it is difficult to compare particulate size distribution and chemical composition changes before and after the size fractionation of the samples. Size fractionation is anticipated to cause retention of smaller particulates in membranes having a larger pore size. These primary particles will overestimate the weight of the filtered sample and underestimate the weight of the next filtration step consisting in a membrane having a smaller pore size. Since particle sieving begins with large-sized particles and finishes with small-sized particles, the magnitude of a_i^* and b_i^* for relatively large (small) particulates is likely to be under-(over-) estimated. Bias on mass of size fractions was verified by comparing the sum of masses for 0.7-10 μm and $>10 \mu\text{m}$ with the total sample filtered through a GF/F filter (i.e., 0.7 μm nominal pore size). The arithmetic average (median) of relative bias for the whole study area was 29.7% (24.9%) or a 29.7% (24.9%) overestimation of mass for particulates $> 0.7 \mu\text{m}$ when total weight is computed based on sum of partial weights corresponding to different size fractions. An optimization scheme to adjust the mass for each size fractions (i.e. adjusting the various masses to sum up to the total mass filtered) was not attempted since we didn't filter total samples through 0.2 or 0.4 μm membranes due to the sequential mode of our filtration. Thus, 'filtration weighting factors' for size fractions $> 0.2 \mu\text{m}$ or $> 0.4 \mu\text{m}$ could not be calculated.

4.5 Optical proxies of particle characteristics

In terms of fractioned mass, the size of particulates was the dominant variable driving changes on γ (ρ_s up to 0.53, $P = 0.004$). Conversely, the mineral content of SPM did not have a statistically detectable impact at 95% confidence interval. In particular, the strongest response of γ to size effects was manifested for the mass fraction having the smallest particulates (i.e., 0.2-0.4 μm). Despite the major effects of particle size classes on γ , values of γ were not clearly correlated with ξ slopes. In oceanic waters, ξ and γ values are expected to covary in a linear way for a specific range of refractive index and ξ (Boss et al., 2001; Twardowski et al., 2001). Our range of ξ values was within the natural variability reported in coastal and oceanic environments ($\xi = 2-4.5$) (Reynolds et al., 2010; Neukermans et al., 2012; Xi et al., 2014). Also, the magnitude of γ in our samples (0.29-2.22 nm^{-1}) was within the range of values that characterize oceanic environments (0.2-2) (Twardowski et al., 2001, Boss et al., 2013). Unlike oceanic waters, the poor correspondence between ξ and γ values in this study was linked to different responses of spectral c_{SPM} and particle size distribution slopes to changes of two non-covarying optical contributions: minerals and phytoplankton. Also, the reduced number of sampling locations and the geographic variability of ξ - γ relationships were additional factors likely explaining the lack of a general functionality for the study area. Lastly, ξ and γ were not substantially correlated in our samples due to deviations on Mie-based models (e.g. absorbing spheres) of γ as a function of ξ (Twardowski et al., 2001). Indeed during our surveys, high absorbing particulates were present in SLE-SF waters.

The variability of S_{vis} values in this study was relatively high (~10-fold) with respect to other littoral environments (1.3-fold, $S_{vis} = 0.009-0.0113 \text{ nm}^{-1}$) (Estepa et al., 2012). No statistically significant correlations at 95% confidence level were computed between F_{SPM}^{PIM} and S_{vis} ($\rho_s = -0.06$, $P = 0.781$). This is counterintuitive as F_{SPM}^{PIM} is strongly correlated to

a_i^* (440) (see Table 2) and presumably iron content of particulates. This discrepancy might be related to the inclusion of freshwater or brackish samples into the correlation analysis as $Svis$ is only expected to change with extractable-iron of measurements made in marine samples (Estapa et al., 2012). Additional correlations between F_{SPM}^{PIM} and $Svis$ values measured in LE locations confirmed this hypothesis ($\rho_s = -0.62$, $P = 0.018$, $N = 14$) and suggest a direct link between PIM content of SPM and a_i^* (440) variations. Likewise as expected, $Svis$ was inversely related a_{SPM}^* (440) in marine waters of the SLE ($\rho_s = -0.55$, $P = 0.04$). Since a_{SPM}^* (440) tends to increase in iron-enriched particulates (Estapa et al., 2012), lower $Svis$ values in LE locations are likely associated with mineral particle assemblages having a greater proportion of iron.

5 Conclusions

The measure of mass-specific optical coefficients of SPM is essential for developing optical inversions and improves our understanding regarding the origin of optical signatures in remote sensing studies and map biogeo-chemical components in surface waters. In this contribution, we presented for the first time, mass-specific scattering and absorption coefficients of size fractionated SPM in estuarine waters of the Saint Lawrence River and a major SLE tributary, the Saguenay Fjord.

Despite the intrinsic variability of weight-normalized optical coefficients due to variations of particle micro-physical attributes, the following patterns were identified: 1. the mass-specific absorption coefficient of SPM was preferentially influenced by changes in particle chemical composition as inferred from changes on F_{SPM}^{PIM} , 2. changes on PSD had a larger impact on b_{SPM}^* with respect to a_{SPM}^* variations, and 3. regional variations on $Svis$ are likely suggesting iron-enrichment of suspended particulates in LE waters.. In summary, these relationships will be useful for investigating local and regionally-limited functionalities and properties of SPM. Without separate independent studies of true optical properties of PSD, the application of the relationships to other littoral environments will remain problematical.

6 Funding

This investigation was supported by the Natural Sciences and Engineering Research Council of Canada, Individual Discovery grant, project title: "Optical remote Sensing models of suspended Particulate matter in the St. Lawrence Estuary "(OSPLE), awarded to Dr. Martin Montes Hugo.

7 Acknowledgements

We thank to the crew of the Creed and Mr. Alexandre Palardy for their assistance during the field work. Also, we appreciate the support of ISMER technicians Mr. Pascal Rioux and Ms. Dominique Lavallée during the field surveys and the processing of lab measurements. Lastly, we are really in debt with the constructive comments of two anonymous reviewers.

References

- Agrawal, Y., McCave I. and Riley J.: Laser diffraction size analysis, in *Principles, Methods, and Application of Particle Size Analysis*, edited by James P. M. Syvitski, pp. 119–129, Cambridge University Press, N. Y., 1991.
- Agrawal, Y. C., A. Whitmire, O. A. Mikkelsen and H. C. Pottsmith H.C.: Light scattering by random shaped particles and consequences of measuring suspended sediments by laser diffraction, *J. Geophys. Res.*, 113, C04023. doi:10.1029/2007JC004403, 2008.
- Andrews, S., D. Nover and S. G. Schladow: Using laser diffraction data to obtain accurate particle size distributions: The role of particle composition, *Limnol. Oceanogr.: Methods* 8, 507–526. doi:10.4319/lom.2010.8.507, 2010.
- Babin, M., Therriault, J.C., Legendre, L. and Condal, A.: Variations in the specific absorption coefficient for natural phytoplankton assemblages: Impact on estimates of primary production, *Limnol. Oceanogr.*, 38, 154-177, 1993.
- Babin, M., Stramski D., Ferrari G.M., Claustre H., Bricaud, A., Obolensky, G. and Hoepffner N.: Variations in the light absorption coefficients of phytoplankton, nonalgal particles, and dissolved organic matter in coastal waters around Europe, *J. Geophys. Res.*, 108, 10.1029/2001JC000882, 2003.
- Babin, M. and Stramski, D.: Variations in the mass-specific absorption coefficient of mineral particles suspended in water, *Limnol. Oceanogr.*, 49, 756–767, 2004.
- Barillé-Boyer, A.L., Barillé, L., Massé, H., Razet, D. and Héral, M: Correction for particulate organic matter as estimated by loss on ignition in estuarine ecosystems, *Estuar. Coast. Shelf Sci.*, 58, 147–153, 2003.
- Bernatchez, P. and Dubois, J.-M. M.: Bilan des connaissances de la dynamique de l'érosion des côtes du Québec maritime laurentien, *Géographie Phys. Quat.*, 58, 45, 2004 (in french).
- Bettiol, C., Stievano, L., Bertelle, M., Delfino, F., and Argese. E.: Evaluation of microwave-assisted acid extraction procedures for the determination of metal content and potential bioavailability in sediments. *Appl. Geochem.* 23, 1140–1151, 2008.
- Binding, C.E., Bowers, D.G. and Mitchelson-Jacob, E.G.: Estimating suspended sediment concentrations from ocean colour measurements in moderately turbid waters; the impact of variable particle scattering properties, *Rem. Sens. Environ.*, 94, 373-383, 2005.
- Boss, E., Twardowski, M.S., and Herring, S.: Shape of the particulate beam attenuation spectrum and its relation to the size distribution of oceanic particles, *App. Opt.* 40, 4885–4893, 2001.
- Boss, E., Slade, H., Behrenfeld, M. and Dall'Olmo, G.: Acceptance angle effects on the beam attenuation in the ocean, *Opt. Expr.*, 17, 1535-1550, 2009.
- Boss, E., Picheral, M., Leeuwa, T., Chase, A., Karsenti, E., Gorsky, G., Taylor, L., Slade, W., Ras, J., Claustre, H.: The characteristics of particulate absorption, scattering and attenuation coefficients in the surface ocean; Contribution of the Tara Oceans expedition, *Methods in oceanography*, 7, 52-62, 2013.

- Bowers, D. G. and Binding, C. E.: The optical properties of mineral suspended particles: A review and synthesis, *Estuar. Coast. Shelf Sci.*, 67, 219–230, 2006.
- Bowers, D.G., Braithwaite, K.M., Nimmo-Smith, W. A. M. and Graham, G. W.: Light scattering by particles suspended in the sea: The role of particle size and density, *Cont. Shelf Res.*, 29, 1748–1755, 2009.
- 5 Bricaud, A. and Stramski, D.: Spectral absorption coefficients of living phytoplankton and nonalgal biogenous matter: A comparison between Peru upwelling area and the Sargasso Sea, *Limnol. Oceanogr.*, 35, 562-582, 1990.
- Chanut, J. P. and Poulet, S. A.: Short-term variability of the size spectra of suspended particles in a rapidly changing environment., *Estuar. Coast. Shelf Sci.*, 15, 497–513, 1982.
- D'Anglejan, B. F. and Smith, E. C.: Distribution, Transport, and Composition of Suspended Matter in the St. Lawrence
- 10 Estuary, *Can. J. Earth Sci.*, 10, 1380–1396, 1973.
- Dalu, T., Richoux, N. B., and Froneman, P. W.: Nature and source of suspended particulate matter and detritus along an austral temperate river-estuary continuum, assessed using stable isotope analysis, *Hydrobiologia*, 767, 95-110, 2016.
- Deflandre B., Mucci, A., Gagne, J.P., Guignard, C., Sundby, and B.: Early diagenetic processes in coastal marine sediments disturbed by a catastrophic sedimentation event. *Geochimica et Cosmochimica Acta*, 66, 2547-2558, 2002.
- 15 Devlin, M. J., Barry, J., Mills, D. K., Gowen, R. J., Foden, J., Sivyer, D., and Tett, P.: Relationships between suspended particulate material, light attenuation and Secchi depth in UK marine waters, *Estuar. Coast. Res. Shelf Sci.*, 79, 429-439, 2008.
- Doxaran, D., Froidefond, J. M., Lavender, S., and Castaing, P.: Spectral signature of highly turbid waters: Application with SPOT data to quantify suspended particulate matter concentrations, *Remote Sens. Environ.*, 81, 149–161, 2002.
- 20 Doxaran, D., Ruddick, K., McKee, D., Gentili, B., Tailliez, D., Chami, M. and Babin, M.: Spectral variation of light scattering by marine particles in coastal waters, from visible to near infrared, *Limnol. Oceanogr.*, 54, 1257–1271, , 2009.
- D'Sa E.J., Miller R.L., and Del Castillo C: Bio-optical properties and ocean color algorithms for coastal waters influenced by the Mississippi River during a cold front, *Appl. Opt.*, 45, 7410–7428, 2006.
- El-Sabh, M.I.: Physical oceanography of the St. Lawrence estuary. In: Kjerfve, B. (Ed.), *Hydrodynamics of Estuaries*.
- 25 *Estuarine Case Studies*, vol. II. CRC Press, Boca Raton, Florida, pp. 61–78, 1988.
- Estapa, M. L., Boss, E., Mayer, L. M. and Roesler, C. S.: Role of iron and organic carbon in mass-specific light absorption by particulate matter from Louisiana coastal waters, *Limnol. Oceanogr.*, 57, 97–112, 2012.
- Fauchot, J., Saucier, F. J., Levasseur, M., Roy, S. and Zakardjian, B.: Wind-driven river plume dynamics and toxic *Alexandrium tamarense* blooms in the St. Lawrence estuary (Canada): A modeling study, *Harmful Algae*, 7, 214–227, 2008.
- 30 Gagné, H., Lajeunesse, P., St-Onge, G. and Bolduc, A.: Recent transfer of coastal sediments to the Laurentian Channel, Lower St. Lawrence Estuary (Eastern Canada), through submarine canyon and fan systems, *Geo-Marine Lett.*, 29, 191–200, 2009.

- Guinder, V. A., Popovich, C. A., and Perillo, G. M. E.: Particulate suspended matter concentrations in the Bahia Blanca Estuary, Argentina: Implication for the development of phytoplankton blooms, *Estuar. Coast. Res. Shelf Sci.*, 85, 157-165, 2009.
- Larouche, P. and Boyer-Villemaire, U.: Suspended particulate matter in the St. Lawrence estuary and Gulf surface layer and development of a remote sensing algorithm, *Estuar. Coast. Shelf Sci.*, 90, 241–249, 2010.
- Levasseur, M., Therriault, J.-C. and Legendre, L.: Hierarchical control of phytoplankton succession by physical factors, *Mar. Ecol. Prog. Ser.*, 19, 211–222, 1984.
- Loisel, H., Nicolas, J. M., Sciandra, A., Stramski, D. and Poteau, A.: Spectral dependency of optical backscattering by marine particles from satellite remote sensing of the global ocean, *J. Geophys. Res. Ocean.*, 111, 1–14, 2006.
- 10 Loisel, H., Duforet, L., Dessailly, D., Chami, M., and Dubuisson, P.: Investigation of the variations in the water leaving polarized reflectance from the POLDER satellite data over two biogeochemical contrasted oceanic areas, *Opt. Exp.*, 17, 12905-12918, 2008.
- Löptien, U. and Meier, H. E. M.: The influence of increasing water turbidity on the sea surface temperature in the Baltic Sea: A model sensitivity study, *J. Mar. Syst.*, 88, 323–331, 2011.
- 15 Ma, H., Kim, S. D., Allen, H. E., and Cha, D. K.: Effect of copper binding by suspended particulate matter on toxicity, *Environ. Toxicol. Chem.* 21, 710-714, 2002.
- Mayer, 1994
- McKee, D., Piskozub, J. and Brown, I.: Scattering error corrections for in situ absorption and attenuation measurements, *Opt. Exp.*, 16, 19480-19492, 2008.
- 20 McKee, D., Piskozub, J., Röttgers, R., Reynolds, R.A.: Evaluation and improvement of an iterative scattering correction scheme for in situ absorption and attenuation measurements, *J. Amer. Ocean. Technol.*, 30, doi.10.1175/JTECH-D-12-00150.1, 2013.
- Miller, R. L. and McKee, B. A.: Using MODIS Terra 250 m imagery to map concentrations of total suspended matter in coastal waters, *Remote Sens. Environ.*, 93, 259–266, 2004.
- 25 Mohammadpour, G., Montes-Hugo, M. A., Stavn, R., Gagné, J. P. and Larouche, P.: Particle Composition Effects on MERIS-Derived SPM: A Case Study in the Saint Lawrence Estuary, *Can. J. Remote Sens.*, 41, 515–524, 2015.
- Montes-Hugo, M. A. and Mohammadpour, G.: Biogeo-optical modeling of SPM in the St. Lawrence Estuary, *Can. J. Remote Sens.*, 38, 197–209, 2012.
- Morel, A. and Antoine, D.: Heating Rate within the Upper Ocean in Relation to its Bio-optical State, *J. Phys. Oceanogr.*, 24, 1652–1665, 1994.
- 30 Neukermans, G., Loisel, H., Mériaux, X., Astoreca, R. and McKee, D.: In situ variability of mass-specific beam attenuation and backscattering of marine particles with respect to particle size, density, and composition, *Limnol. Oceanogr.*, 57, 124–144, 2012.

- Neukermans, G., Reynolds, R. A. and Stramski, D.: Optical classification and characterization of marine particle assemblages within the western Arctic Ocean, *Limnol. Oceanogr.*, 61, 1472–1494, 2016.
- Nieke, B., Reuter, R., Heuermann, R., Wang, H., Babin, M. and Therriault, J. C.: Light absorption and fluorescence properties of chromophoric dissolved organic matter (CDOM), in the St. Lawrence Estuary (Case 2 waters), *Cont. Shelf Res.*, 17, 235–252, 1997.
- Pearson, R.K.: Mining imperfect data. Dealing with contamination and incomplete records. Society for Industrial and Applied Mathematics, 305 p. doi.org/10.1137/1.9780898717884, 2005.
- Pegau, W.S., Gray, D., and Zaneveld, J.R.V.: Absorption and attenuation of visible and near-infrared light in water: Dependence on temperature and salinity, *Appl. Opt.*, 36, 6035–6046, 1997.
- 10 Poulet, S., Cossa, D. and Marty, J.-C.: Combined analyses of the size spectra and biochemical composition of particles in the St. Lawrence estuary, *Mar. Ecol. Prog. Ser.*, 30, 205–214, 1986.
- Poulton, S.W., and Raiswell R.: Chemical and physical characteristics of iron oxides in riverine and glacial meltwater sediments, *Chem. Geol.*, 218, 203–221, 2005.
- Ramalhosa, E., Pereira, E., Vale, C., Válega, M., Monterroso, and P., Duarte, A. C.: Mercury distribution in Douro estuary (Portugal), *Mar. Poll. Bull.* 50, 1218–1222, 2005.
- 15 Reynolds, R.A., Stramski, D., Wright, V.M., and Woźniak, S.B.: Measurements and characterization of particle size distributions in coastal waters, *J. Geoph. Res.*, 115, doi:10.1029/2009JC005930, 2010.
- Reynolds, R. A., Stramski, D. and Neukermans, G.: Optical backscattering by particles in Arctic seawater and relationships to particle mass concentration, size distribution, and bulk composition, *Limnol. Oceanogr.*, 61, 1869–1890, 2016.
- 20 Risovic, D.: Two component model of the sea particle size distribution, *Deep-Sea Res., Part I*, 40, 1459–1473, 1993.
- Röttgers, R., Schönfeld, W., Kipp, P.R., and Doerffer, R.: Practical test of a point-source integrating cavity absorption meter: The performance of different collector assemblies, *App. Opt.*, 44, 5549–5560, 2005.
- Röttgers, R., McKee, D., and Woźniak, S. B.: Evaluation of scatter corrections for ac-9 absorption measurements in coastal waters, *Methods Oceanogr.*, 7, 21–39, 2013.
- 25 Röttgers, R., Dupouy, C., Taylor, B. B., Bracher, A. and Woźniak, S. B.: Mass-specific light absorption coefficients of natural aquatic particles in the near-infrared spectral region, *Limnol. Oceanogr.*, 59, 1449–1460, 2014.
- Slade, W.H., Boss, E. and Russo C.: Effects of particle aggregation and disaggregation on their inherent optical properties, *Opt. Exp.*, 19, 7945–7959, 2011.
- Snyder, W., Arnone, R., Davis, C. O., Goode, W., Gould, R. W., Ladner, S., Lamela, G., Rhea, W. J., Stavn, R., Sydor, M. and Weidemann, A.: Optical scattering and backscattering by organic and inorganic particulates in U.S. coastal waters., *Appl. Opt.*, 47, 666–77, 2008.
- 30 Spearman, C.: The Proof and Measurement of Association between two things, *The Amer. J. of Psych.*, 15, 1904.
- Stavn, R. H. and Richter, S. J.: Biogeo-optics: particle optical properties and the partitioning of the spectral scattering coefficient of ocean waters., *Appl. Opt.*, 47, 2660–2679, 2008.

- Tremblay, L. and Gagné, J. P.: Distribution and biogeochemistry of sedimentary humic substances in the St. Lawrence Estuary and the Saguenay Fjord, Québec, Org. Geochem., 38, 682–699, 2007.
- Tremblay, L. and Gagné, J. P.: Organic matter distribution and reactivity in the waters of a large estuarine system, Mar. Chem., 116, 1–12, 2009.
- 5 Twardowski, M.S., Boss, E., Macdonald, J.B., Pegau, W.S., Barnard, A.H. and Zaneveld J.R.V.: A model for estimating bulk refractive index from the optical backscattering ratio and the implications for understanding particle composition in case I and case II waters, J. Geophys. Res, 106, C7, 14,129-14,142, 2001.
- Wóźniak, S. B., Stramski, D., Stramska, M., Reynolds, R. A., Wright, V. M., Miksic, E. Y., Cichocka, M. and Cieplak, A. M.: Optical variability of seawater in relation to particle concentration, composition, and size distribution in the nearshore
 10 marine environment at Imperial Beach, California, J. Geophys. Res. Ocean., 115, 1–19, 2010.
- Xi, H., Larouche, P., Tang, S. and Michel, C.: Seasonal variability of light absorption properties and water optical constituents in Hudson Bay, Canada, J. Geophys. Res. Ocean., 118, 3087–3102, 2014.
- Xie, H., Aubry C., Bélanger S., and Song G.: The dynamics of absorption coefficients of CDOM and particles in the St. Lawrence estuarine system: Biogeochemical and physical implications, Mar. Chem., 128-129, 44-56, 2012.
- 15 Yeats, P. A.: The distribution of trace metals in ocean waters, Sci. Total Environ., 72, 131–149, 1988.
- Yeats, P. A. and Bowers, J. M.: Trace metals in the waters of the Saguenay Fjord, Can. J. Earth Sci., 13, 1319–1327, 1976.
- Zaneveld, J.R.V., Kitchen, J.C., Moore, C.M.: The scattering correction error of the reflecting-tube absorption meters, Ocean Optics XII, J.S. Jaffe, Ed. International Society for Optical Engineering, SPIE proceedings, vol. 2258, 44-58, 1994.
- Zhang, X., Huot, Y., Gray, D.J., Weidemann, A., and Rhea, W.J.: Biogeochemical origins of particles obtained from the
 20 inversion of the volume scattering function and spectral absorption in coastal waters, Biogeosciences, 10, 6029e6043, 2013.
- Zhang, X., Stavn, R. H., Falster, A. U., Gray, D. and Gould, R. W.: New insight into particulate mineral and organic matter in coastal ocean waters through optical inversion, Estuar. Coast. Res. Shelf Sci., 149, 1–12, 2014.
- Zhang, X., Stavn, R.H., Falster, A.U., Rick, J.J., Gray, D. and R.W. Gould, Jr.: Size distributions of coastal ocean suspended particulate inorganic matter: Amorphous silica and clay minerals and their dynamics, Estuar., Coast. and Shelf Sci.. DOI:
 25 10.1016/j.ecss.2017.03.025, 2017.

Table 1. Summary of acronyms

Abbreviation	Definition	Unit
SLE	St. Lawrence Estuary	
UE	Upper Estuary	
SF	Saguenay Fjord	
LE	Lower Estuary	
CSPM	Concentration of suspended particulate matter	g m^{-3}
F_{SPM}^i	Contribution of size fraction i to total mass of SPM	dimensionless
F_{SPM}^j	Contribution of chemical fraction j to total mass of SPM	dimensionless
NAP	Non-algal particulates	
CDOM	Chromophoric dissolved organic matter	
λ	Light wavelength	nm
a_{SPM}	Absorption coefficient of total SPM	m^{-1}
b_{SPM}	Scattering coefficient of total SPM	m^{-1}
c_{SPM}	Particulate beam attenuation coefficient of total SPM	m^{-1}
a_{SPM}^*	Mass-specific absorption coefficient of total SPM	$\text{m}^2 \text{g}^{-1}$
b_{SPM}^*	Mass-specific scattering coefficient of total SPM	$\text{m}^2 \text{g}^{-1}$
ξ	Differential Junge slope of particle size distribution	Number of particulates per μm
D	Diameter of a volume-equivalent sphere at mid point of size class	μm

V(D)	Volume concentration at size class D	$\mu\text{L L}^{-1}$
N(D)	Particle number concentration at size class D	m^{-3}
N'(D)	Particle number density at size class D	$\text{m}^{-3} \mu\text{m}^{-1}$
γ	Spectral slope of particulate beam attenuation coefficient	nm^{-1}
S_{vis}	Spectral slope of mass-specific particulate absorption coefficient within the visible spectral range	nm^{-1}

5

10

15

20

Table 2. Particle size and chemical composition effects on mass-specific optical coefficients. Spearman rank correlations for a_i^* and b_i^* are computed at a wavelength of 440 and 550 nm, respectively.

Mass-specific	ξ	$F_{\text{SPM}}^{\text{PIM}}$
Optical fraction		
$a_{0.2-0.4 \mu\text{m}}^*$	0.32 *	0.31 *
$a_{0.4-0.7 \mu\text{m}}^*$	0.28 *	0.50 **
$a_{0.7-10 \mu\text{m}}^*$	0.26 *	0.49 *
$a_{>10 \mu\text{m}}^*$	0.31 *	0.44 *
$b_{0.2-0.4 \mu\text{m}}^*$	0.15	-0.17 *
$b_{0.4-0.7 \mu\text{m}}^*$	0.05	-0.06
$b_{0.7-10 \mu\text{m}}^*$	0.23 *	0.42 *
$b_{>10 \mu\text{m}}^*$	0.37 *	0.26 *

5

10

Table 3. Correlation of optical proxies with mass-derived size and chemical fractions of SPM. Spearman rank correlations based on 23 samples.

Mass fraction of particulates	γ	<i>Svis</i>
$F_{\text{SPM}}^{\text{PIM}}$	-0.34	-0.06
$F_{\text{SPM}}^{0.2-0.4 \mu\text{m}}$	0.53*	0.49**
$F_{\text{SPM}}^{0.4-0.7 \mu\text{m}}$	-0.43*	-0.49**
$F_{\text{SPM}}^{0.7-10 \mu\text{m}}$	-0.38*	-0.30*
$F_{\text{SPM}}^{>10 \mu\text{m}}$	0.13	0.19

5

10

Table 4. Mass-specific optical coefficients of suspended particulates for different littoral environments. Acronyms and units are defined in Table 1.

Location	λ	a_{SPM}^*	b_{SPM}^*	CSPM ⁱ	References
UE	440	0.01 – 0.25 ^a	0.01 – 1.06 ^a	2.28 – 30.6	This study
	488	0.01 – 0.14	0.01 – 0.97		
	556	0.01 – 0.06	0.01 – 0.86		
	665	0.01 – 0.02	0.01 – 0.73		
	708	0.01 – 0.012	0.01 – 0.68		
SF	440	0.32 - 0.73	0.20-0.56		
	488	0.17 - 0.39	0.18-0.49		
	556	0.08 – 0.17	0.15-0.42		
	665	0.02 – 0.04	0.13 – 0.34		
	708	0.01 – 0.02	0.12 – 0.31		
LE	440	0.03 – 0.07	0.04 – 0.22		
	488	0.02 – 0.04	0.04 – 0.21		
	556	0.01 – 0.02	0.04 – 0.19		
	665	0.003 – 0.006	0.04 – 0.18		

	708	0.015 – 0.002	0.04 – 0.17		
Elber River,	650	0.001 – 0.020 ^b		0.5-10	Röttgers et al. (2014)
German Bight,	750	0.001 – 0.019			
Baltic Sea, New Caledonia lagoon	850	0.001 – 0.014			
Monterey Bay, US	532		0.46 – 2.54 ^c	0.11 – 2.37	Zhang et al. (2014)
Mobile Bay, US	532		0.40 – 1.78	0.26 – 7.36	
Mobile Bay,	440	0.44 – 1.95 ^d		0.23-25.32	Stavn and Richter (2008)
Southwest Pass, US	488	0.41 – 1.89			
	550	0.40 – 1.80			
	676	0.36 – 1.63			
	715	0.34 – 1.61			
Coast of New Jersey,	440			0.44 – 6.6	Snyder et al. (2008)
Monterey Bay,	488				
Great Bay	556				
Mobile Bay	665	0.05 ± 0.01 ^d (arithmetic			

		mean standard deviation)	±			
Irish sea, UK	665		0.08 – 0.45 ^e	1.9 – 26.5	Binding et al. (2005)	
Irish sea, UK	443	0.062 ± 0.013 ^f	0.17 – 0.19	1.6 – 50	Bowers and Binding (2006)	
	490		0.20 – 0.22			
	555		0.20 – 0.24			
	665		0.14 – 0.15			
Coast off Europe and French Guyana	676		0.63 – 2.07 ^g	1.2 – 82.4	Neukermans et al. (2012)	
Elbe Estuary, Germany	555	0.05 – 0.07 ^d	0.35 – 0.47	73.5 – 294.2	Doxaran et al. (2009)	
	715	0.01 – 0.03	0.32 – 0.44			
Gironde Estuary, France	555	0.02 – 0.06	0.28 – 0.50	21.9 – 344.1		
	715	0.01 – 0.02	0.27 – 0.45			
Coastal Louisiana and lower Atchafalaya and	440	0.056 ± 0.012 ^g (0.05 - 0.065)			Estapa et al. (2012)	

Mississippi Rivers

488	0.035 - 0.05
556	0.25 - 0.35
665	0.125 - 0.02

West of Mississippi
Delta

443	0.012 - 0.079 ^d
-----	----------------------------

D'Sa et al. (2006)

Imperial Beach,
California

440	0.03 - 0.1 ^h	0.1 - 1.2	3-90
488	0.02 - 0.08	0.18 - 0.9	
556	0.01 - 0.03	0.2 - 0.9	
665	0.004 - 0.02	0.2 - 0.8	
708	0.001 - 0.02	0.2 - 0.8	

Wozniak et al. (2010)

^aac-s measurements and sum of weights of SPM size fractions 0.2-0.4 μm, 0.4-0.7 μm, 0.7-10 μm and >10 μm, ^bintegrating sphere coupled to spectrophotometer for suspensions and pad-technique, SPM weight based on GF/F (pore size = 0.7 μm) and nucleopore Whatman (pore size = 0.4 μm) filters, ^cMultispectral volume scattering meter and optical models for different particle subpopulations with asymmetrical shape, ^dac-9 measurements and SPM weight based on GF/F filters, ^eIrradiance meter PRR600 and optical models for estimating inherent optical properties and SPM weight based on GF/F filters, ^fcomparable to ^cbut pad-technique for estimating absorption coefficients of SPM, ^gcomparable to ^d but using ac-s measurements, ^hcomparable to ^b but using only suspensions and weight based on GF/F filters, ⁱcomparable to ^b but using only GF/F filters for SPM weight, ⁱconcentration of SPM for particulates >0.7 μm.

Figure captions

Figure 1. Study area. UE (green triangles), LE (blue rectangles) and SF (red circles). GSL is the Gulf of St. Lawrence.

5 Figure 2. Spectral variation of mass-specific optical coefficients for total SPM. (a) particulate absorption at $\lambda = 440$ nm, (b) particulate scattering at $\lambda = 550$ nm. Each bar is the arithmetic average ± 2 standard errors as computed for different regions of the study area. Number of observations for UE, SF and LE are 3, 5 and 15 respectively.

Figure 3. Spectral variation of mass-specific absorption coefficients for different size classes of suspended particulates. (a) 0.2-0.4 μm , (b) 0.4-0.7 μm , (c) 0.7-10 μm and (d) >10 μm . Curves presenting negative values at some wavelengths are not depicted. SF (black line), UE (red line) and LE (blue line).

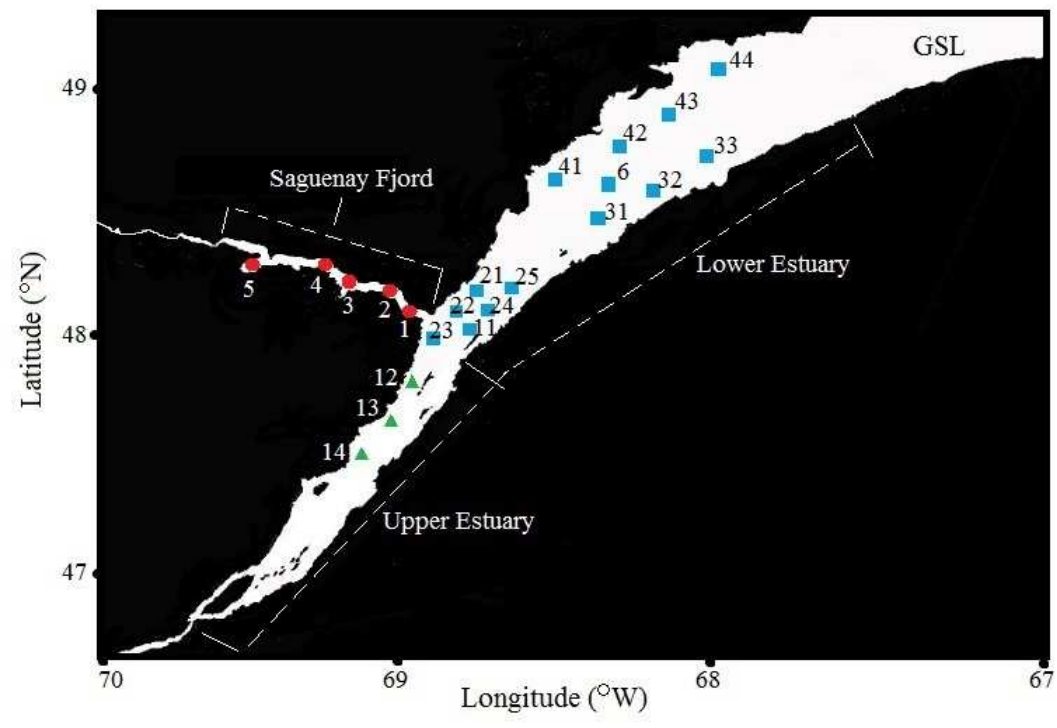
10 Figure 4. Spectral variation of mass-specific scattering coefficients for different size classes of suspended particulates. Symbols of size classes idem as Fig. 3. Curves presenting negative values at some wavelengths are not depicted

Figure 5. Mass-specific optical coefficients for size fractions of SPM and as a function of wavelength. (a) particulate absorption, (b) particulate scattering . Each bar is the arithmetic average ± 2 standard errors. as computed over the whole study area.

15 Figure 6. Subregional variation of mass-specific optical coefficients for size fractions of SPM . (a) particulate absorption at $\lambda = 440$ nm, (b) particulate scattering at $\lambda = 550$ nm. Each bar is the arithmetic average ± 2 standard errors as computed for each spatial domain.

20

25



5
fig. 1

10

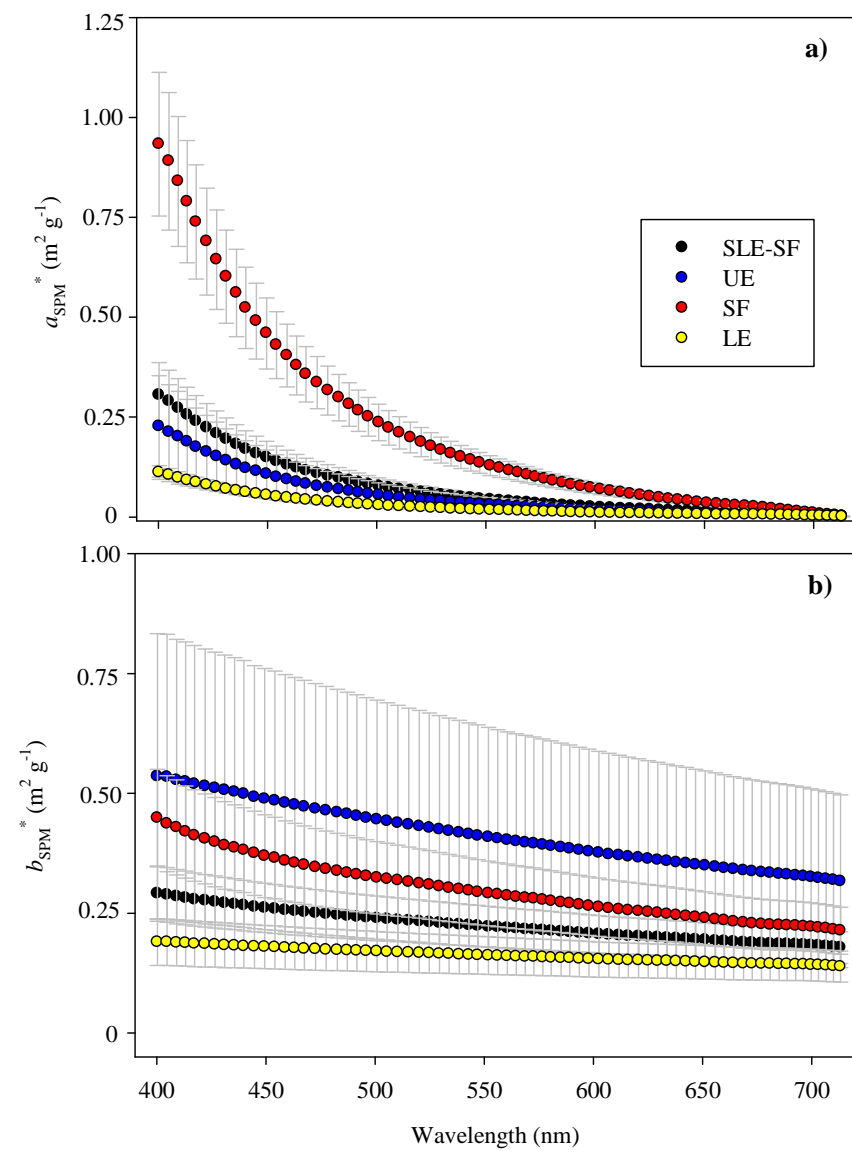
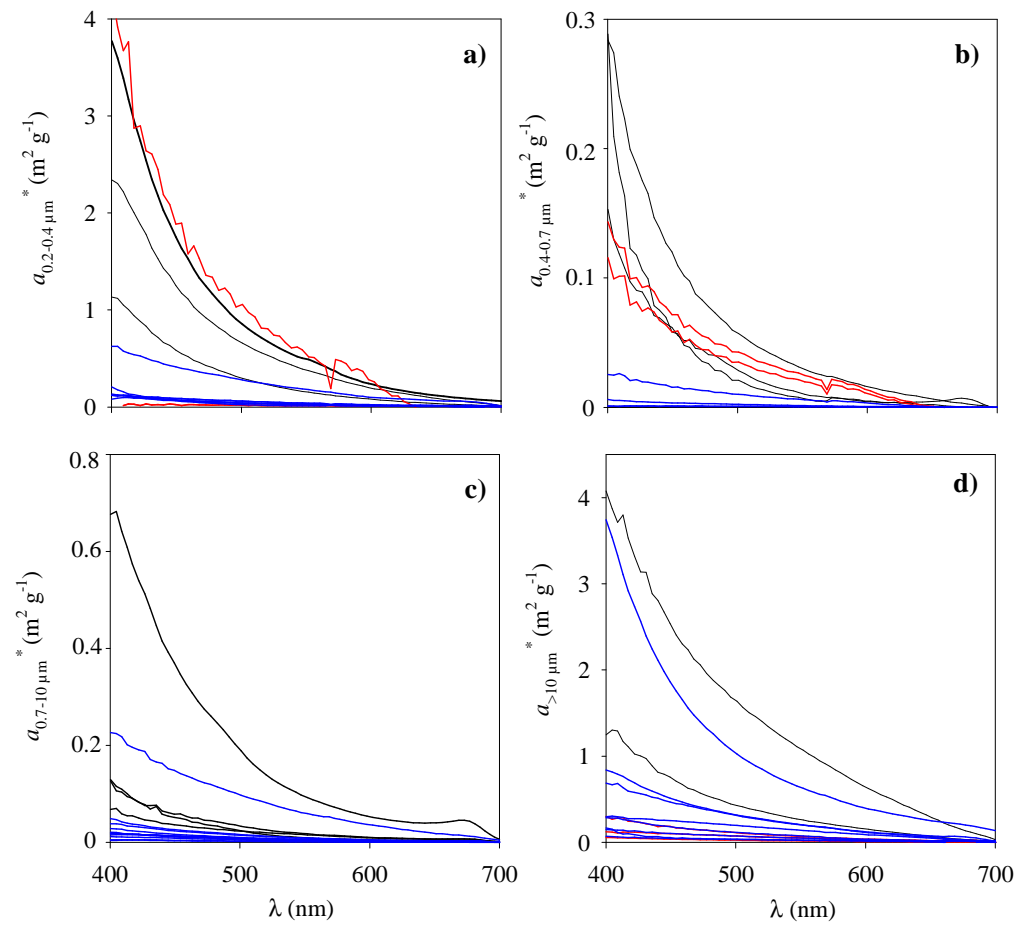
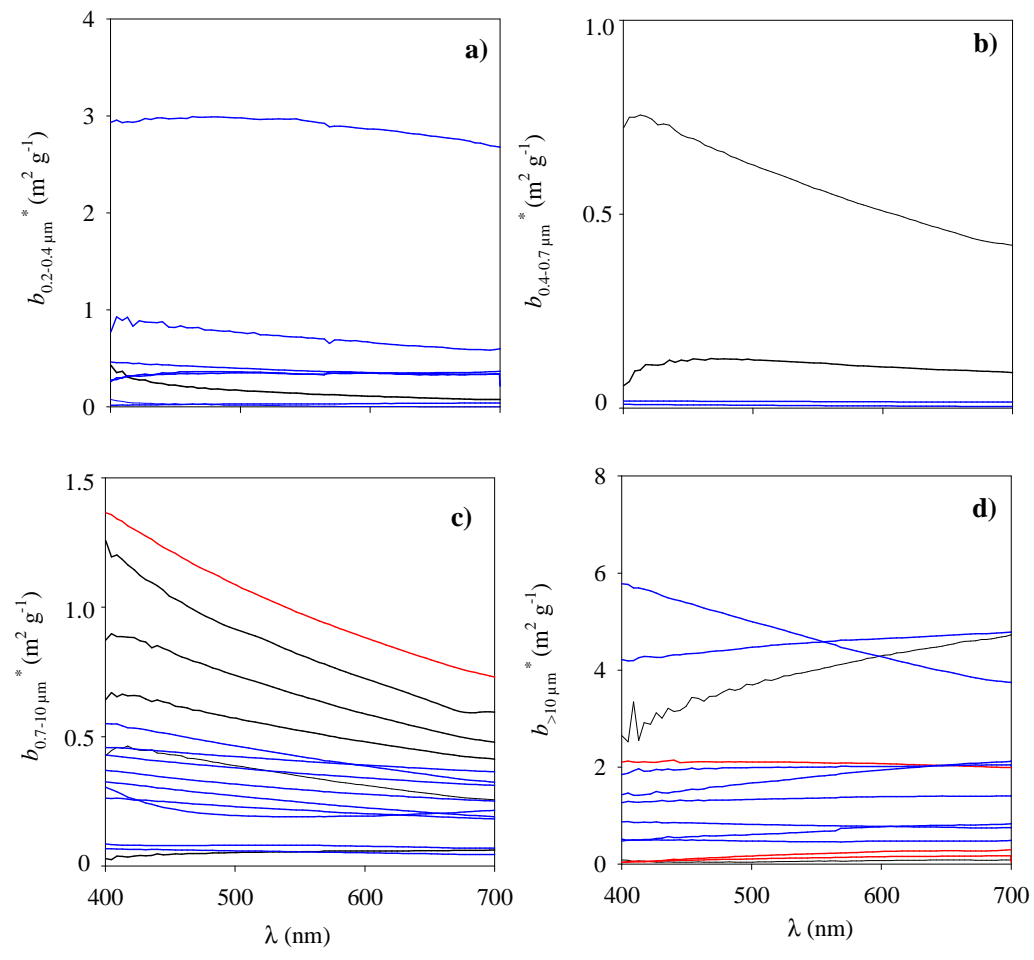


Fig. 2



5 Fig. 3

10



5 Fig. 4

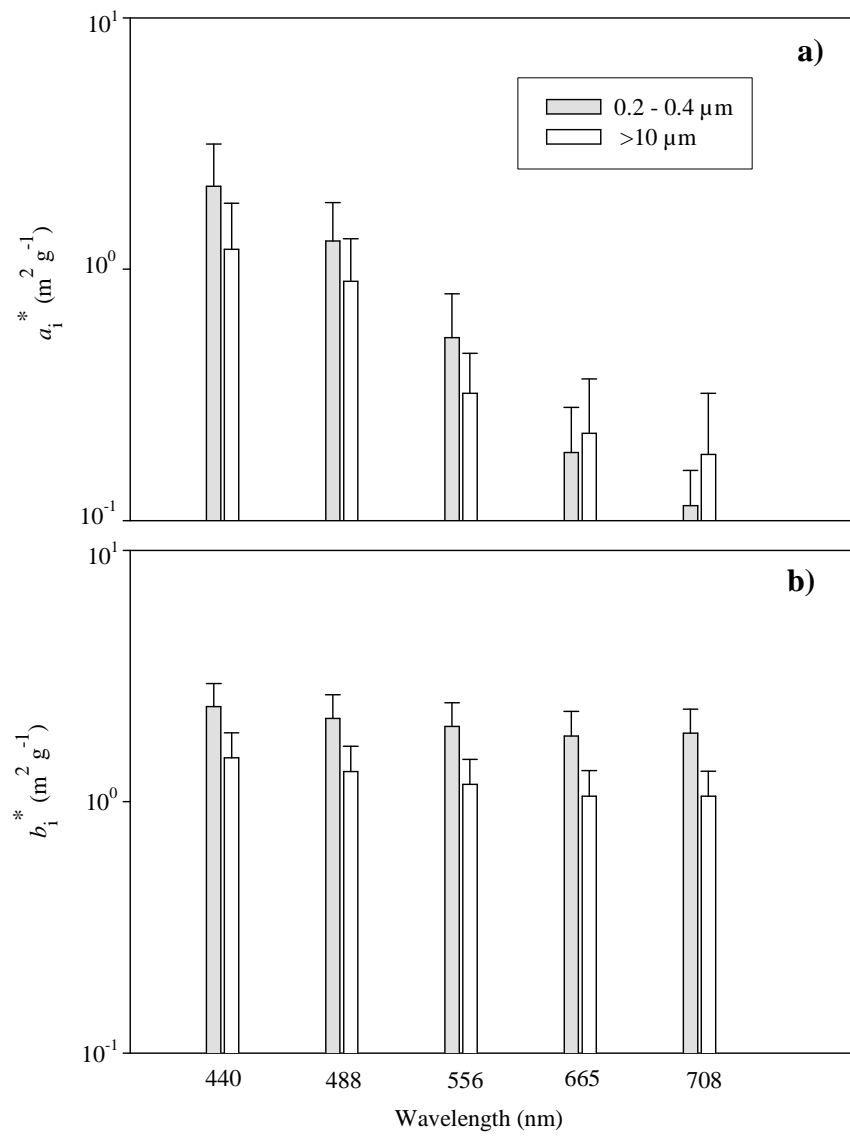


fig. 5

5

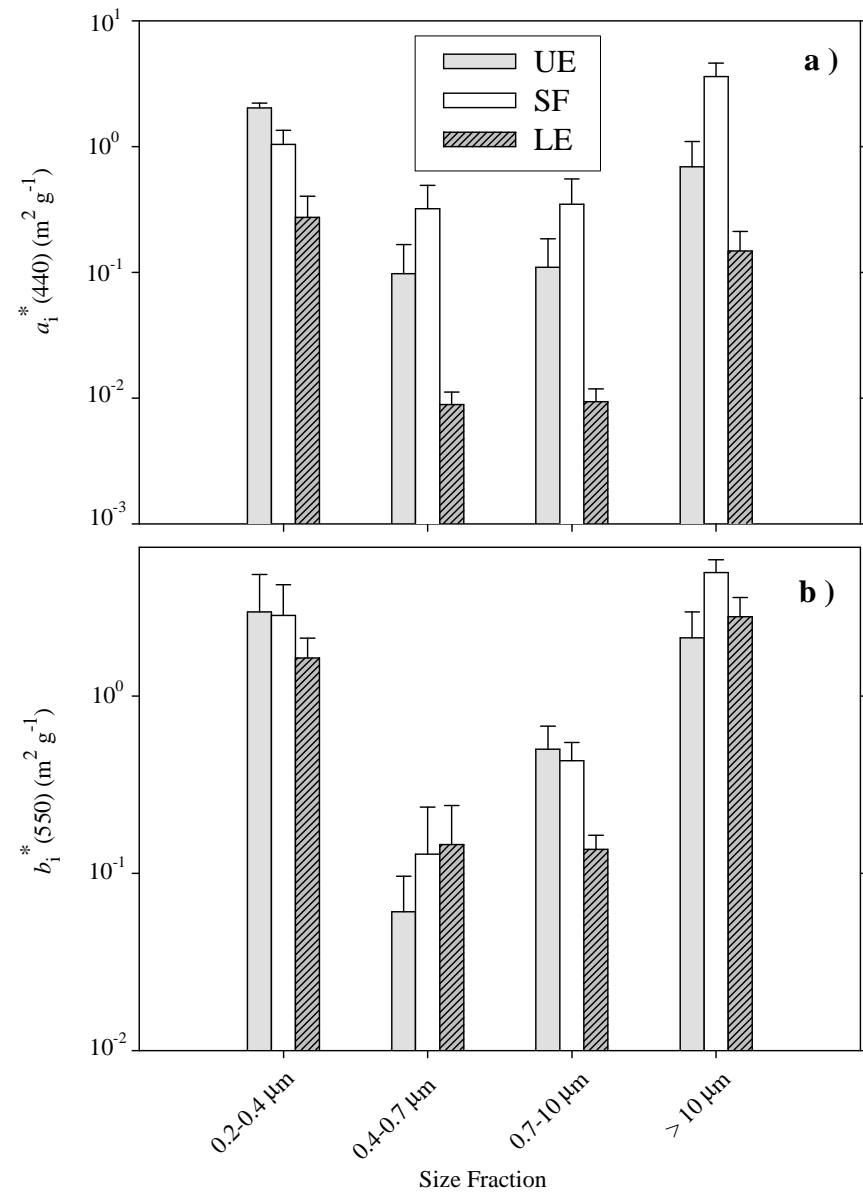


Fig. 6